

University of Groningen

Hybrid organic spin valves

Popinciuc, Mihaita

IMPORTANT NOTE: You are advised to consult the publisher's version (publisher's PDF) if you wish to cite from it. Please check the document version below.

Document Version

Publisher's PDF, also known as Version of record

Publication date:

2007

[Link to publication in University of Groningen/UMCG research database](#)

Citation for published version (APA):

Popinciuc, M. (2007). *Hybrid organic spin valves: interfaces and transport*. s.n.

Copyright

Other than for strictly personal use, it is not permitted to download or to forward/distribute the text or part of it without the consent of the author(s) and/or copyright holder(s), unless the work is under an open content license (like Creative Commons).

The publication may also be distributed here under the terms of Article 25fa of the Dutch Copyright Act, indicated by the "Taverne" license. More information can be found on the University of Groningen website: <https://www.rug.nl/library/open-access/self-archiving-pure/taverne-amendment>.

Take-down policy

If you believe that this document breaches copyright please contact us providing details, and we will remove access to the work immediately and investigate your claim.

Downloaded from the University of Groningen/UMCG research database (Pure): <http://www.rug.nl/research/portal>. For technical reasons the number of authors shown on this cover page is limited to 10 maximum.

Energy level alignment at Co/AlO_x/Pentacene interfaces¹

X-ray and ultraviolet photoelectron spectroscopy (XPS and UPS) experiments were performed in order to study the energy level alignment and electronic structure at Co/AlO_x/pentacene interfaces as a function of the aluminium oxide (AlO_x) tunnel barrier thickness and the oxidation state of Co. XPS was used to determine the oxygen exposure for the optimum oxidation of 6, 8 and 10 Å thin layers of Al deposited on Co. The Fermi level (FL) position in the band gap of AlO_x depends on the oxidation state of the underlying Co and on the thickness of the tunnel barrier. The energy level alignment at Co/AlO_x interfaces is consistent with an interfacial dipole, its magnitude being sensitive to the oxidation of Co, and band bending phenomena in the thin AlO_x tunnel barrier. UPS experiments revealed no chemical interaction at the Co/AlO_x/pentacene interface in contrast with hybridization effects found at Co/pentacene interface. The vacuum level of pentacene aligns with that of AlO_x, following the position of AlO_x energy levels with respect to FL. The hole injection barrier was found to increase with the thickness of the tunnel barrier and to decrease with the degree of oxidation of Co at a fixed thickness of the AlO_x layer. This enables tuning the performance of pentacene based spin valves by controlling the thickness of the tunnel barrier.

¹Published as: M. Popinciuc, H. T. Jonkman, and B. J. van Wees, *J. Appl. Phys.*, **101**, 093701 (2007)

5.1 Introduction

All electrical spin injection and detection in semiconductors (organic or inorganic) using ferromagnetic metals (such as Co) suffer from a common problem: the conductivity mismatch problem [1]. Theoretical predictions suggest that the problem can be solved by the insertion of thin tunnel barriers (e.g. aluminium oxide) in between the ferromagnetic metal and the semiconductor [1, 2]. Depending on the conductivity of the organic material, tuning of the tunnel barrier resistance by its thickness, is generally required. Whether the tunnel barrier influences (and how) the energy level alignment scheme at Co/AlOx/pentacene interfaces is not known. Up to date there are no studies (photoemission or transport) regarding the carrier injection barriers at Co/AlOx/pentacene interfaces. The insertion of thin insulating layers of LiF in between an organic semiconductor and metal contacts have shown to improve the performance of organic LEDs [3–5]. The effect was explained by the modification of the carrier injection barriers, information inferred from photoelectron spectroscopy experiments [6–10].

In this chapter we present photoelectron spectroscopy experiments of the interfacial energy level alignment between Co and pentacene in the case of the insertion of a thin aluminium oxide (AlOx) tunnel barrier in between. The tunnel barriers were fabricated by oxidation of thin (6, 8 and 10 Å) layers of Al deposited on Co. The oxidized silicon substrates were liquid nitrogen cooled in order to assure a smooth surface and a closed Al layer. The aluminium layers were oxidized by exposing the sample in steps to oxygen (99.5 %) at room temperature. XPS spectra were acquired after each exposure step. The oxidation state of Al and the oxygen exposure for which the Al layers are optimally oxidized were obtained from XPS measurements by analyzing the binding energy (BE) and full width half maximum (FWHM) of the Al 2*p* and Al 2*s* core levels. Next, UPS experiments were performed as a function of pentacene thickness deposited on optimally oxidized Co/AlOx substrates in order to deduce the interfacial energy level alignment. More experimental details were described in *Section 3.3*.

5.2 Al oxidation monitored by XPS and UPS

In Fig. 5.1 a few spectra (normalized and displaced vertically) in the region of Al 2*p*, Al 2*s* and Co 2*p* core levels are presented for the oxidation of 6 Å Al deposited on 25 Å Co. The Co layer was intentionally kept thin in order to improve the sensitivity in detecting its oxidation at the interface with AlOx. The oxygen exposure is expressed in Langmuirs (L), 1 L = 1.33 × 10⁻⁶ mbar·sec. Similar spectra were taken for all samples (6, 8 and 10 Å Al).

The energy levels of Al shift towards higher BE as the Al metal undergoes

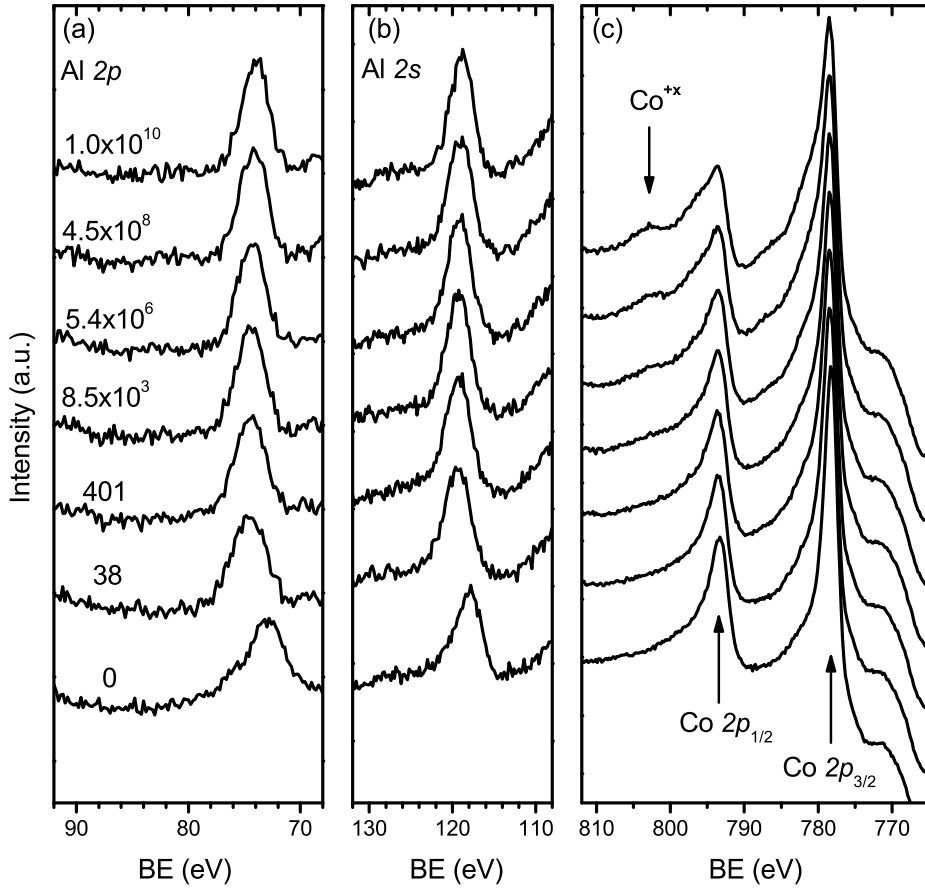


Figure 5.1: A few XPS spectra of 6 Å Al metal on Co at different oxygen exposure doses (the numbers represent the total oxygen exposure expressed in langmuirs and are valid for all the traces, from bottom to top). a) Al 2*p*, b) Al 2*s* and c) Co 2*p* regions. Note the shift of Al energy levels and the broadening of Co 2*p* by the appearance of oxidized cobalt levels (Co^{+*x*}) with increasing the oxygen exposure dose.

oxidation, that is the chemical state of Al changes from Al⁰ in neutral Al metal to Al³⁺ in Al₂O₃ [11]. In the beginning of the oxidation process Al is present in a mixture of pure and oxidized Al. This is reflected in the width of Al 2*p*, Al 2*s*, see bottom spectra of Fig. 5.1(a)-(b). The resolution of our spectrometer did not allowed to clearly separate two energy levels, one of pure Al and one of oxidized Al, so fitting of the data was done assuming only one gaussian function and a Shirley type of background [11]. We will show later that in spite of this

restriction we are able to determine the optimum oxidation conditions without any doubt. The BE and FWHM of Al $2p$ were tracked as a function of total oxygen exposure and the results obtained from fitting are shown in Fig. 5.2 for all samples (6, 8 and 10 Å Al). The Al $2s$ level evolves similar to Al $2p$. At low oxygen exposures the FWHM is larger with respect to a pure or completely oxidized Al layer owing to the mixture of pure and oxidized Al. After a certain oxygen exposure the FWHM saturates, consistent with the existence of only one oxidation state of Al. Further oxygen exposure does not change the chemical state of Al, therefore we consider that the optimum oxidation is when FWHM saturation starts, that is 140, 0.9×10^6 and 10^{10} L for the 6, 8 and 10 Å Al layers, respectively. Beyond this point the underlying Co starts to oxidize, that is, Co $2p$ energy levels broaden as oxidized Co (Co $^{+x}$) energy levels develop in the spectra, see Fig. 5.1(c). In a separate experiment we exposed a clean Co surface to oxygen and found that Co readily oxidizes (*Section 3.3.2*). This is in contrast with the late appearance of cobalt oxide (CoOx) signs in the case the deposition of the 6 Å Al layer, indicating a good coverage of the surface by the Al layer. Roughly, the saturation in FWHM corresponds to a peak in BE for the Al energy levels, which we interpret as an extra indication that the underlying Co layer starts to oxidize.

Fig. 5.3 summarizes the XPS results of Al core levels of the AlOx tunnel barriers as a function of the initial Al layer thickness (d). In all plots presented in this chapter we represent the variable thickness of AlOx by the initial thickness of Al from which the tunnel barrier was derived. To obtain the thickness of the oxide barrier d should be multiplied by a factor of ~ 1.2 assuming the bulk densities of Al and γ -Al $_2$ O $_3$. In Fig. 5.3(a) we present the binding energy shift of the levels with respect to d . Within less than a tenth of the experimental resolution the Al core levels have a constant binding energy. The FWHM of Al $2p$ and Al $2s$ (average values taking all the points in the saturation region) is shown in Fig. 5.3(b). Within the error bars, which represent the standard deviation, the FWHM is constant.

The following phenomena may take place at the Co/AlOx interface: formation of interfacial dipole, chemistry (pinning), screening effects, band bending, intermixing of Al with Co and charging. We can exclude charging effects in XPS from the following two reasons. First, charging should broaden the energy levels with increasing the insulating layer thickness whereas we found FWHM to be constant. Secondly, charging should be more severe with the appearance of the CoOx layer in between Co and AlOx and should shift the energy levels of Al towards higher binding energies, which is actually opposite to what we observed. This is in agreement with previous reports which showed that charging does not occur in aluminium oxide layers thinner than 25 Å [12, 13]. Intermixing of Al

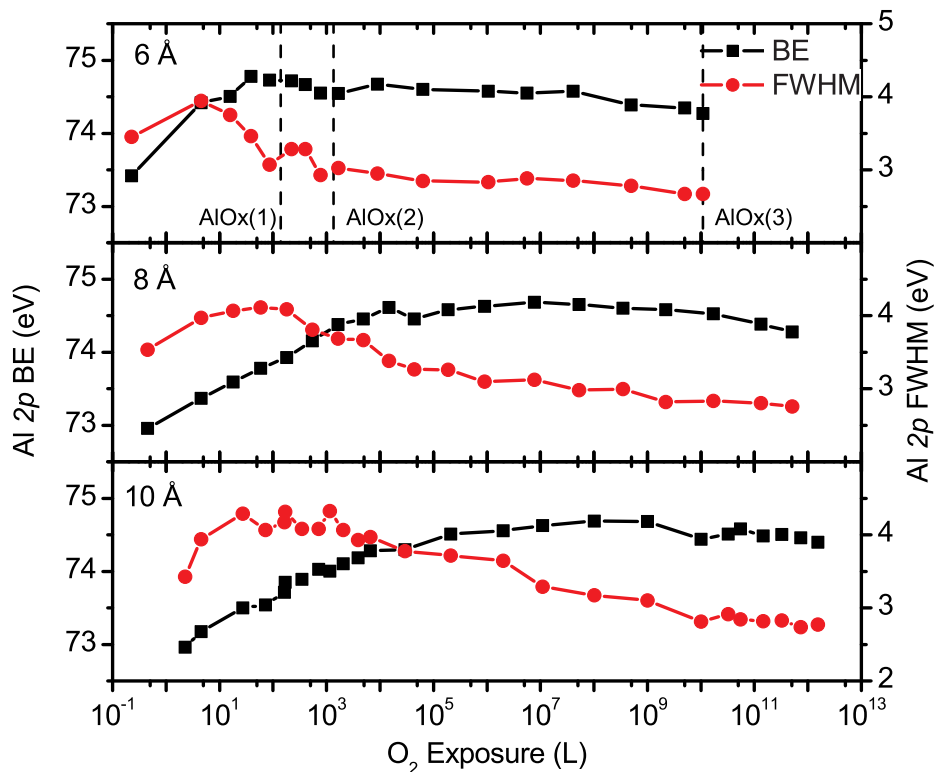


Figure 5.2: The BE (squares, left axis) and FWHM (circles, right axis) of Al 2p energy level as a function of oxygen exposure for (from top to down) 6, 8 and 10 Å Al on Co. The vertical dashed lines represent the oxygen exposures of the three samples (6 Å Al) for which the pentacene energy level alignment was measured by UPS, as discussed later in Sec. 5.4.

and Co species cannot play a major role for the following reason. Very likely, the intermixed AlOx layer would have a different FWHM compared with a pure one due to non-uniformities in the chemical environment. In fact the FWHM should peak at the point where the probed layer consists of equal quantities of intermixed Co-AlOx and pure AlOx layers. Our data show a constant FWHM (within the error bars), therefore pointing to a uniform chemical environment and to a sharp Co/AlOx interface. This is also consistent with the late appearance of Co oxidation signs which points to a good coverage and small intermixing of Al with Co. Screening effects, due to close proximity of the Co metal do not have a significant contribution since the Al levels shift towards lower BEs with the appearance of CoOx layer (which increases the distance between Co metal and

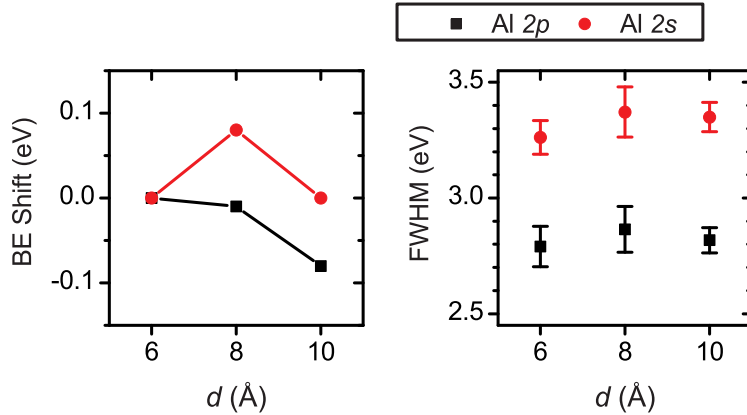


Figure 5.3: (a) Binding energy shift and (b) FWHM of Al 2p (squares) and Al 2s (circles) as a function of the initial Al layer thickness.

AlOx), contrary to what it would be expected if metal screening would play a major role. Different FL positions with respect to a common VL of Co and AlOx lead to an interfacial dipole at Co/AlOx interface, whose magnitude is affected by the interfacial states present at Co/AlOx interface. With the appearance of a thin CoOx layer in between Co and AlOx the nature of these interfacial states is changed and a change in the magnitude of the interfacial dipole is expected to occur, in agreement with the change (decrease) of the BE of Al core levels.

UPS spectra of optimum oxidized layers were also recorded, Fig. 5.4(a). We identify the broad feature around 6.5 eV as corresponding to the valence band of aluminium oxide. In Figs. 5.4(b)-(c) we show the position of the top of the valence band with respect to FL (denoted as VB) as a function of oxidation state of Co and as a function of the initial Al layer thickness (d). As already discussed, at the Co/AlOx interface an interfacial dipole exists and its magnitude is sensitive to the oxidation state of the underlying Co. The UPS data also show a decrease in the binding energy of the VB with oxidizing Co, in agreement with the XPS measurements (see Figs. 5.2). As a function of d , an increase in BE of the VB is observed in UPS in contrast with the XPS measurements. A possible explanation is a stronger differential charging in the UPS measurements, which we cannot completely exclude. However, literature data on thin aluminium oxide layers grown on various metals [13–16] showed an increase of the Al core levels binding energies with increasing the thickness of the oxide as well. Thin insulating layers of LiF deposited on metals behave similarly [7, 17]. The shift towards higher binding energies of the energy levels of the insulating layer with increasing the insulator thickness was interpreted in most cases in terms of interfacial dipole,

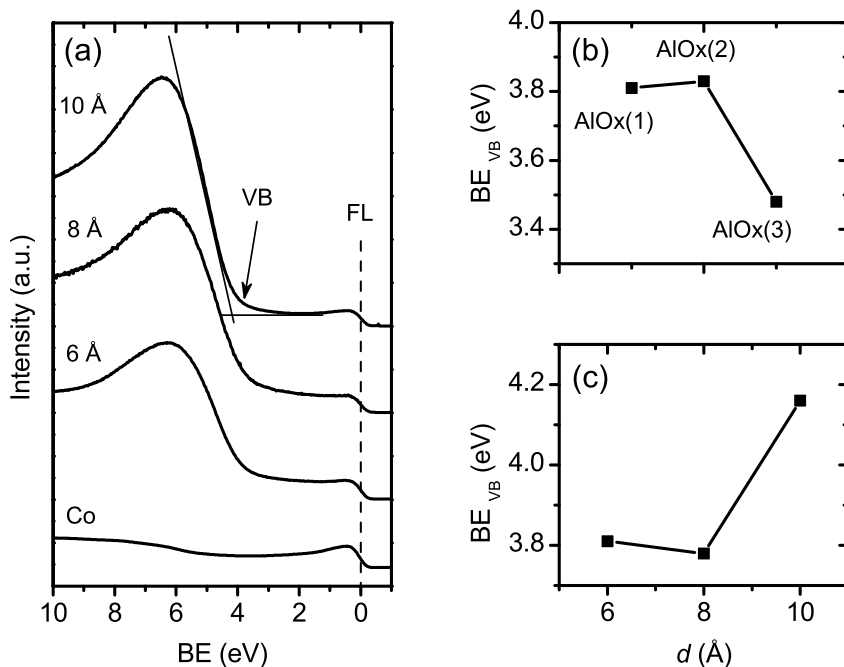


Figure 5.4: (a) UPS spectra of optimum oxidized Al layers showing the top of valence band of AlOx (VB). (b) the BE of VB (BE_{VB}) as a function of the oxidation of Co for the 6 Å sample (see text). (c) BE of VB of AlOx as a function of initial thickness of the Al layer, d .

Schottky barrier formation and band bending in the thin insulating layer. Taking into account the discussion of the XPS data in the previous paragraph we believe that the energy level alignment at Co/AlOx interface is due to Schottky barrier formation and band bending in the AlOx layer.

5.3 Energetics of Co/AlOx/pentacene vs. Co/pentacene interfaces

In this section we present the results on the energetics of the Co/AlOx/pentacene interfaces. A comparison is made with the clean contact case, Co/pentacene.

In the clean contact case between pentacene and Co there is a high degree of interaction [18, 19] as shown in the previous chapter. Due to hybridization of the highest molecular orbital (HOMO) of pentacene with the reactive Co $3d$ band, the BE of HOMO level was found to be higher for the interfacial layer (submonolayer

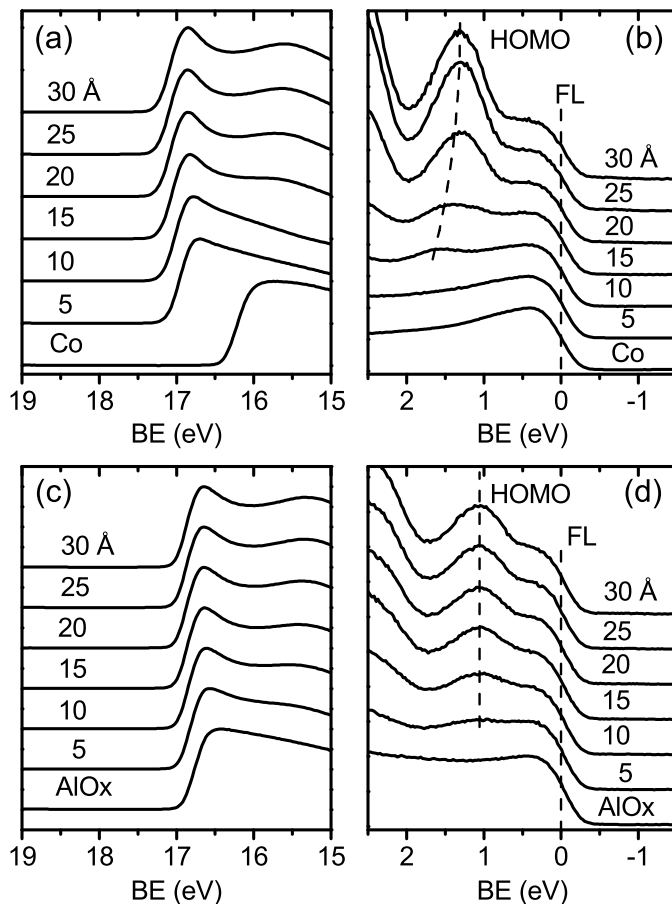


Figure 5.5: (a) and (b) UPS spectra of pentacene deposited on Co in the region of secondary electron cut-off and Fermi level, respectively. (c) and (d) UPS spectra in the case of insertion of an optimum oxidized 6 Å Al layer between Co and pentacene. The dashed lines are a guide to the eyes and represent the FL and the evolution of HOMO level with increasing pentacene coverage.

coverage of pentacene) in comparison with the two monolayer (≈ 30 Å) coverage situation. This is illustrated in Fig. 5.5(b) where we present the measured UPS spectra in the region of HOMO for a few thicknesses of pentacene. In the case of insertion of AlOx tunnel barrier in between Co and pentacene there is no chemical interaction, as the BE of HOMO level stays approximately the same for the interfacial layer compared with a thicker film, see Fig. 5.5(d). Note that in the clean contact case at 5 Å pentacene coverage the HOMO level is not de-

tectable, whereas when the tunnel barrier is inserted the HOMO level becomes visible. This behavior was consistent in all samples employing an AlOx tunnel barrier, indicating no chemical activity for Co/AlOx/pentacene system compared with Co/pentacene, in agreement with measurements on the Al/AlOx/pentacene system [20]. The hole injection barrier (the distance between leading edge of HOMO and the FL) amounts to 1.0 eV for Co/pentacene interface, whereas for Co/AlOx(6 Å)/pentacene interface the barrier height is 0.6 eV for the tunnel barrier derived from oxidizing 6 Å Al. At the Co/pentacene interface we found an interfacial dipole of 1.1 eV, whereas for the Co/AlOx(6 Å)/pentacene system we found an interfacial dipole of 0.7 eV at the Co/AlOx interface and vacuum level alignment at the AlOx/pentacene interface. A vacuum alignment situation was reported also for SiO₂/pentacene and LiF/pentacene interfaces [17, 21].

5.4 Energy level alignment at Co/AlOx/Pentacene interfaces

In this section we discuss the variation of the hole injection barrier (Δ_h) as a function of the oxidation state of the underlying Co (for the 6 Å Al samples) and as a function of the thickness of the tunnel barrier (the optimum oxidized 6, 8 and 10 Å Al layers). The hole injection barrier and vacuum level alignment were determined for each of the samples. All samples show a similar behavior, that is VL alignment of pentacene with the AlOx tunnel barrier and constant HOMO binding energy with increasing thickness of pentacene consistent with no interfacial chemical reaction between pentacene and AlOx as previously discussed.

From the organic spin valve devices point of view it is important that Co is not oxidized at the interface with the AlOx tunnel barrier. In order to investigate to what extent the oxidation of the Co underlayer influences the hole injection barrier at Co/AlOx/pentacene interface we prepared three similar samples (same 6 Å thickness of Al) and performed UPS measurements. The difference between the samples was in the oxygen dose at which the Al layer was exposed. The oxygen exposure conditions for the three samples are indicated in Fig. 5.2 by the vertical dashed lines. The samples were denoted as: optimum oxidized AlOx(1), slightly over-oxidized AlOx(2) and over-oxidized AlOx(3) with corresponding exposures of 140, 1400 and 1×10^{10} L. For optimum oxidized 6 Å Al sample the hole injection barrier is smaller than in the clean contact case between Co and pentacene and decreases even more with the oxidation of Co. In Fig. 5.6(a) we plotted the variation of Δ_h together with the binding energy shifts of VL (at Co/AlOx interface) and Al 2*p*, Al 2*s*, for the three samples. The variable thickness samples show that Δ_h increases with the oxide thickness and amounts to: 0.6 eV, 0.7 eV and 0.9 eV

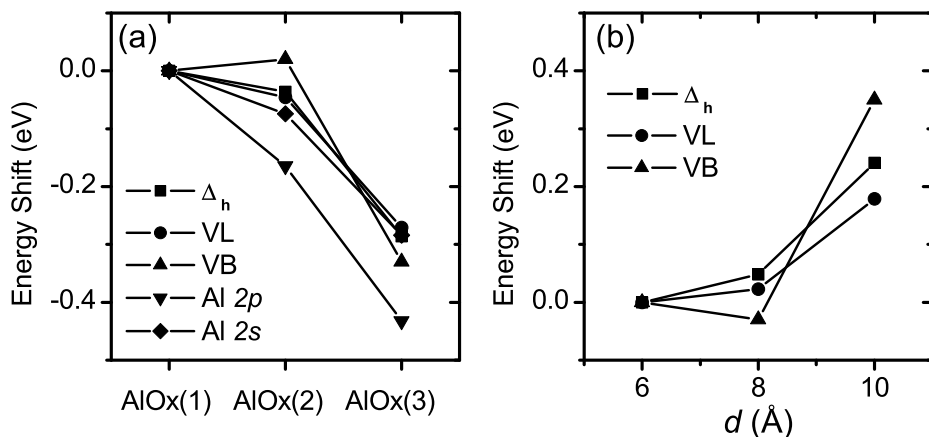


Figure 5.6: (a) the variation of Δ_h and binding energy shifts of VL (at the Co/AlOx interface), VB of AlOx, Al 2p and Al 2s for the three, differently oxidized, 6 Å Al samples. The hole injection barrier decreases with the oxidation of the underlying Co. (b) the variation of Δ_h and binding energy shifts of VL (at the Co/AlOx interface) and VB as a function of the initial Al layer thickness, d . The hole injection barrier increases as a function of d .

for the 6, 8 and 10 Å Al layers. In Fig. 5.6(b) we plotted the variation of: Δ_h , BE of VL (at Co/AlOx interface) and BE of the VB of AlOx as a function of d .

The hole injection barrier, that is the HOMO level, follows the energy levels of AlOx (Al 2p, Al 2s, VB) in all cases. The difference between samples is the position of the FL at the interface, i.e. the work function of the substrate, determined by the oxidation of Co and/or the thickness of AlOx. A vacuum level alignment situation (the Schottky-Mott limit) was found at all interfaces between Co/AlOx substrates and pentacene, i.e. the band alignment scheme is not determined by the position of the FL in the band gap of the aluminium oxide tunnel barrier. In line with recent efforts to describe the interface energetics of organic semiconductor with various substrates [22,23], the Co/AlOx/pentacene interfaces can be characterized as weakly interacting. The charge transfer between Co and pentacene through the (transparent) AlOx barrier, due to the electrochemical potential equilibration, does not have a major contribution in determining the energy levels alignment at Co/AlOx/pentacene interface, that is the interfacial slope parameter is unity.

5.5 Conclusions

The evolution of Al energy levels, in thin AlOx tunnel barriers, as a function of the oxidation of the underlying Co and as a function of the aluminium oxide thickness were interpreted as due to a combination of two factors: interfacial dipole and band bending. The energetics of Co/AlOx interface determines the band offsets and the magnitude of the interfacial dipole, which decreases with the oxidation of Co. The vacuum levels of pentacene and Co/AlOx substrates were found to align, a situation which corresponds to the Schottky-Mott limit. Charge transfer through the thin tunnel barriers (due to electrochemical potential equilibration) does not play a significant role in determining the energy levels alignment scheme. The hole injection barrier decreases with the oxidation of the bottom Co layer and increases with the thickness of aluminium oxide, following the shift of Al energy levels with respect to FL. This demonstrates that the carrier injection barriers (holes and electrons) can be tuned by varying the oxide barrier thickness. Moreover, we showed that with the insertion of a thin AlOx tunnel barrier (the 6 Å Al case) the hole injection barrier decreases by ~ 0.4 eV compared with the clean contact case and an improvement in the efficiency of injecting holes is expected to occur in electrical devices. The contact resistance of Co/AlOx/pentacene devices is expected to increase with the tunnel barrier thickness due to the following reasons. First, as the aluminium oxide becomes thicker less carriers are able to tunnel through and second, at the same time, the carriers experience a higher injection barrier. Since the magnitude of the hole injection barrier is important in the modeling of the spin valves, the information gained from our experiments will help to successfully model and design pentacene spin valves employing Co and AlOx tunnel barriers.

References

- [1] G. Schmidt, D. Ferrand, L. W. Molenkamp, A. T. Filip, and B. J. van Wees, *Phys. Rev. B* **62**, R4790 (2000)
- [2] A. Fert and H. Jaffres, *Phys. Rev. B* **64**, 184420 (2001)
- [3] L. S. Hung, C. W. Tang, and M. G. Mason, *Appl. Phys. Lett.* **70**, 152 (1997)
- [4] G. E. Jabbour, Y. Kawabe, S. E. Shaheen, J. F. Wang, M. M. Morrell, B. Kippelen, and N. Peyghambarian, *Appl. Phys. Lett.* **71**, 1762 (1997)
- [5] S. E. Shaheen, G. E. Jabbour, M. M. Morrell, Y. Kawabe, B. Kippelen, M.-F. Nabor, R. Schlaf, w. A. Mash, and N. R. Armstrong, *J. Appl. Phys.* **84**, 2324 (1998)
- [6] T. Mori, H. Fujikawa, S. Tokito, and Y. Taga, *Appl. Phys. Lett.* **73**, 2763 (1998)
- [7] R. Schlaf, B. A. Parkinson, P. A. Lee, K. V. Nebesny, G. Jabbour, B. Kippelen, N. Peyghambarian, and N. R. Armstrong, *J. Appl. Phys.* **84**, 6729 (1998)
- [8] Q. T. Le, L. Yan, Y. Gao, M. G. Mason, D. J. Giesen, and C. W. Tang, *J. Appl. Phys.* **87**, 375 (2000)
- [9] G. Greczynski, F. Fahlman, and W. R. Salaneck, *J. Chem. Phys.* **113**, 2407 (2000)
- [10] M. G. Mason, C. W. Tang, L.-S. Hung, P. Raychaudhuri, J. Madathil, D. J. Giesen, L. Yan, Q. T. Le, Y. Gao, S.-T. Lee, et al., *J. Appl. Phys.* **89**, 2756 (2001)

-
- [11] S. Hüfner, Photoelectron spectroscopy (Springer-Verlag, Berlin, 1995).
 - [12] T. L. Barr, *J. Vac. Sci. Technol. A* **7**, 1677 (1989)
 - [13] T. L. Barr, S. Seal, L. M. Chen, and C. C. Kao, *Thin Solid Films* **253**, 277 (1994)
 - [14] Y. Wu, E. Garfunkel, T. E. Madey, and N. D. Shinn, *Surf. Sci.* **336**, 123 (1995)
 - [15] Y. Wu, E. Garfunkel, and T. E. Madey, *Surf. Sci.* **365**, 337 (1996)
 - [16] Y. Yamauchi, M. Yoshitake, and W. Song, *Appl. Surf. Sci.* **273**, 363 (2004)
 - [17] N. J. Watkins and Y. Gao, *J. Appl. Phys.* **94**, 1289 (2003)
 - [18] M. Popinciuc, H. T. Jonkman, and B. J. van Wees, *J. Appl. Phys.* **100**, 93714 (2006)
 - [19] M. V. Tiba, W. J. M. de Jonge, B. Koopmans, and H. T. Jonkman, *J. Appl. Phys.* **100**, 93707 (2006)
 - [20] N. J. Watkins, S. Zorba, and Y. Gao, *J. Appl. Phys.* **96**, 425 (2004)
 - [21] N. J. Watkins and Y. Gao, *J. Appl. Phys.* **94**, 5782 (2003)
 - [22] H. Vázquez, R. Oszwaldowski, P. Pou, J. Ortega, R. Pérez, F. Flores, and A. Kahn, *Europhys. Lett.* **65**, 802 (2004)
 - [23] C. Tengstedt, W. Osikowicz, W. R. Salaneck, I. D. Parker, C.-H. Hsu, and M. Fahlman, *Appl. Phys. Lett.* **88**, 53502 (2006)